
# Compact Heat Exchangers with Curved Fins for Hydrogen Turbofan Intercooling

**Proceedings of ASME Turbo Expo 2024**
**Turbomachinery Technical Conference and Exposition**
**GT2024**
**June 24-28, 2024, London, United Kingdom**

**GT2024-125591**

# COMPACT HEAT EXCHANGERS WITH CURVED FINS FOR HYDROGEN TURBOFAN INTERCOOLING

**Alexandre Capitao Patrao, Isak Jonsson, Carlos Xisto**

Chalmers University of Technology, Gothenburg, SE-41296, Sweden

## ABSTRACT

*Hydrogen is being considered as a possible path towards carbon-neutral aviation. There are additional advantages besides its main benefit of $CO_2$-free combustion. One application is to use it for aero engine heat management due to its cryogenic temperature and high heat capacity, including intercooling and exhaust heat recuperation. The focus of this paper is on the design of a compact heat exchanger integrated into an intermediate compressor duct (ICD), which could decrease compression work and specific fuel consumption (SFC). This compact heat exchanger features curved fins to promote flow turning and decrease pressure losses compared to more conventional straight fin heat exchangers. Conceptual design and duct shape optimization has been carried out which produced integrated ICD heat exchanger designs with significantly lower air-side total pressure losses compared to their conventional straight fin counterparts, which could improve system level integration and engine performance. A direct outcome of this study is a pressure loss correlation which can be used in future engine system level trade studies.*

Keywords: Hydrogen, heat exchangers, intercooling, optimization.

## 1 NOMENCLATURE

| | |
|---|---|
| A | Area [m$^2$] |
| $\alpha_{air}$ | Total air-side transfer area/total volume $[1/m]$ |
| AR | Area Ratio |
| BPR | Bypass ratio |
| $D_h$ | Air-side hydraulic diameter $[m]$ |
| $\Delta R/L$ | Shape factor of the ICD |
| $\epsilon$ | Heat exchanger effectiveness |
| $f$ | Friction factor |
| FPR | Fan pressure ratio |
| $G$ | Mass flux $[kg/m^2 s]$ |
| GA | Genetic Algorithm |
| HEX | Heat Exchanger |
| HPC | High Pressure Compressor |
| ICD | Intermediate compressor duct |
| $K$ | Inertial resistance factor $[1/m]$ |
| $k$ | Thermal conductivity $[W/m\,K]$ |
| $\kappa$ | Fin metal angle |
| $L_x$ | HEX length in air direction $[m]$ |
| $L_y$ | HEX length in H2 direction $[m]$ |
| $L_z$ | HEX length in circumferential direction $[m]$ |
| LHS | Latin Hypercube Sampling |
| LPC | Low Pressure Compressor |
| NTU | Number of Transfer Units |
| OPR | Overall Pressure Ratio |
| $p$ | Pressure [Pa] |
| $Q$ | Heat flow [W] |
| $\dot{q}$ | Volumetric heat source $[W/m^3]$ |
| RBF | Radial Basis Functions |
| $\rho$ | Density $[kg/m^3]$ |
| SFC | Specific Fuel Consumption |
| $\sigma_{air}$ | Free-flow area/frontal area |
| TO | Take-off |
| ToC | Top-of-climb |
| $v$ | Velocity $[m/s]$ |
| $V$ | Volume $[m^3]$ |
| $W$ | Mass $[kg]$ |
| $\xi_{fin}$ | Fin area/total area |

## 2 INTRODUCTION

Hydrogen is currently being evaluated as a potential sustainable fuel option for aviation. Its main advantage compared to hydrocarbons, CO2-free combustion, constitutes a step on the path towards reducing greenhouse gas emissions from aviation. Society-wide efforts to reduce anthropogenic climate change such as the European Green Deal, which aims at achieving an economy with no net greenhouse gas emissions by 2050 [1], are ongoing and supported by large research programs such as Horizon Europe, whose aim includes the development, maturing, and adoption of hydrogen for energy systems [2] and transport [3].

Hydrogen offers several advantages beyond the aforementioned ability to undergo CO2-free combustion; it features higher gravimetric energy density and cooling capacity compared to kerosene-based jet fuels. However, there are challenges associated with using hydrogen in conventional aircraft, primarily due to its relatively lower density and the

 

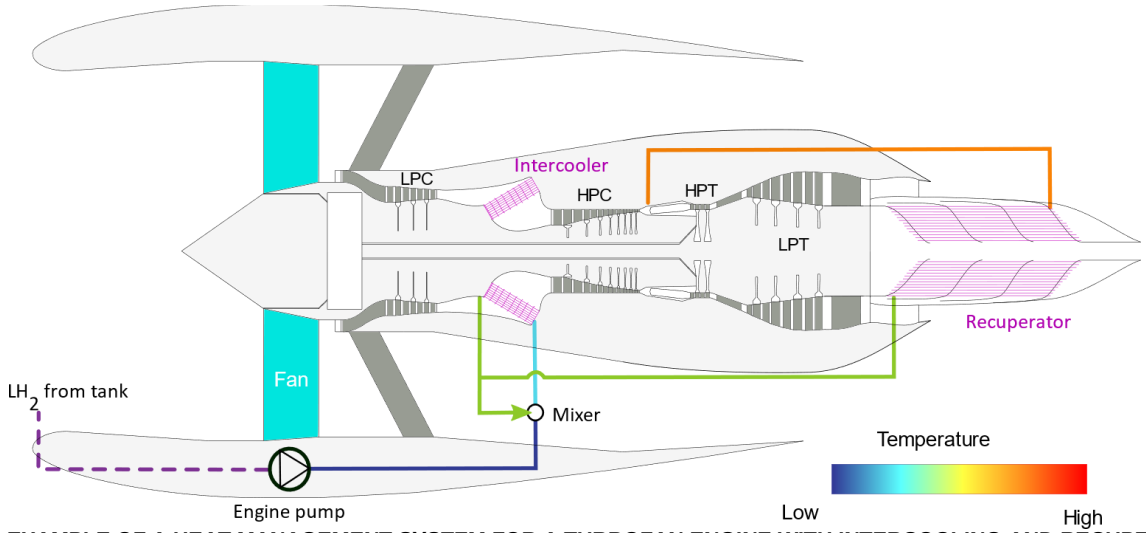


**FIG. 1 - EXAMPLE OF A HEAT MANAGEMENT SYSTEM FOR A TURBOFAN ENGINE WITH INTERCOOLING AND RECUPERATION.**

requirement for cryogenic storage temperatures. These factors impact the size, weight, and insulation of the propellant feed system [4]. On the other hand, the cryogenic storage temperature and high specific heat capacity of hydrogen enables it to be used as a heat sink in the engine [5–10]. The cooling capacity of cryogenic hydrogen is substantial and could lead to significant reductions in specific fuel consumption (SFC). For example, by increasing the hydrogen temperature from 25 K to 800 K before combustion, the absorbed energy content per kilogram of fuel reaches approximately 10% of the fuel's heating value. In a theoretically loss-free system, this alone has the potential to decrease engine-specific fuel consumption by the same amount [11].

Hydrogen can be used for intercooling and/or recuperation, as shown in Fig. 1. *Intercooling* involves cooling in the intermediate compressor duct (ICD) between the low-pressure compressor (LPC) and high-pressure compressor (HPC) ([11,13]). Additionally, there is also *continuous cooling* during the compression process which offers the most significant performance improvement but is characterized by a higher level of complexity [6–8]. *Recuperation* with hydrogen captures heat in the exhaust gases of the engine, by means of cooled vanes or heat exchangers in the turbine rear structure (TRS), which is then injected into the combustion chamber.

Intercooling has the potential to decrease the amount of compression work required in the aero engine. Furthermore, it also allows to increase the engine overall pressure ratio or to decrease the combustor inlet temperature, hence introducing additional degrees of freedom towards improving efficiency and/or decreasing NOx emissions. This has been previously investigated by the authors [9] by employing compressor stators for heat transfer, where each stator vane contains an internal cooling circuit composed of numerous small cooling channels adjacent to the outer vane surface. This approach showed a favorable impact on engine performance, with a specific fuel consumption (SFC) reduction of up to 0.8% and NOx emissions decrease of 3.6%. While high heat transfer rates per unit area were possible in compressor vanes, the impact on engine performance was constrained by the limited available wetted area in the low-pressure compressor.

Incorporating compact heat exchangers into the ICD (see Fig. 2) provides a way to increase the amount of available surface area for heat transfer but requires careful integration of the heat exchangers and connecting ducts to avoid excessive pressure loss, weight, and volume. This was investigated by the authors in [14], which carried out conceptual design, analysis, and optimization of a conical heat exchanger integrated into an ICD duct. This configuration consists of a *diffuser* which decreases the dynamic pressure of the flow, a conical *heat exchanger* (HEX) composed of finned flat tubes, and a *contraction* which routes the air to the HPC inlet. Engine system level calculations for this design incorporated into a hydrogen-fueled turbofan engine showed SFC reductions of 3.9% at take-off and 2.7% at cruise, relative to a non-intercooled reference. It is noted that the improvements were mainly credited to fuel pre-heating. At the same time, due to a reduction in combustor inlet temperatures, NOx emissions were reduced by 34% at take-off and 24% at cruise. The air-side total pressure drop incurred in the ICD ranged between 8 and 9% depending on operating point, of which the vast majority (~60%) could be attributed to flow separation near the inlet of the heat exchanger due to a large incidence angle between the flow and the heat exchanger fins. This represents a clear area for improvement which can further enhance overall engine performance.

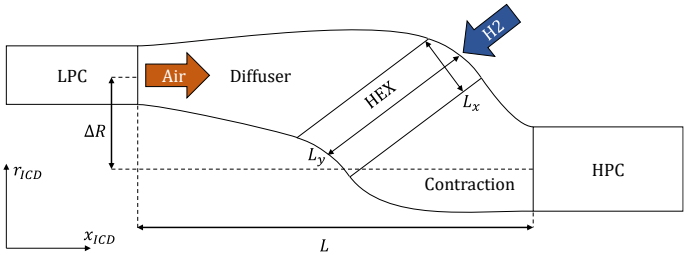


**FIG. 2 - MERIDIONAL VIEW OF A CURVED FIN HEAT EXCHANGER INTEGRATED INTO THE ICD DUCT.**

Consequently, the aim of this paper will be to investigate the aerodynamic performance of an ICD duct containing a heat exchanger with curved fins instead of the more conventional straight fins found in tubed fin heat exchangers, aiming at increasing flow turning, decreasing the pressure losses in the ICD, and improving engine performance. The paper encompasses heat exchanger conceptual design, duct design and optimization, and generation of pressure loss correlations.

## 3 METHODOLOGY

The methodology of this paper can be summarized in the following steps:

1. Heat exchanger conceptual design – Calculating the overall dimensions and performance of the heat exchanger.
2. Duct design and aerodynamic optimization – Integration of the heat exchanger into an ICD duct and subsequent optimization by means of CFD, surrogate modelling, and genetic algorithms. This will be carried out both for heat exchangers with straight and curved fins.
3. Generation of pressure loss correlations – A selected design from the aerodynamic optimization is used for generating pressure loss correlations suitable for engine system level calculations.

These steps will be described in greater detail in subsequent sections.

### 3.1 Heat exchanger conceptual design

Placing a compact heat exchanger in the (relatively) high Mach number flow in an ICD will result in large pressure losses [11]. As mentioned earlier, the flow needs to be diffused first in order to decrease its dynamic pressure, which will decrease the total pressure loss of the core air when it flows through the heat exchanger. An example of such an ICD geometry is shown in Fig. 2 for a curved fin heat exchanger. The air flows from left to right, first along a straight annular channel, corresponding to the hub and shroud endpoints of the LPC outlet. It is followed by the *diffuser* duct, a *heat exchanger* (HEX), and then a *contraction* which connects to the downstream HPC. The area ratio (AR) between the diffuser duct inlet and outlet dictates which Mach number can be obtained at the heat exchanger inlet assuming a well-functioning diffuser with low losses. For this paper, an area ratio of 4 was chosen which together with an LPC outlet design Mach number of 0.4 leads to a Mach number below 0.1 at the inlet of the HEX, constituting a compromise between ICD volume and air-side total pressure losses.

The employed HEX matrix geometry is based on the finned flat tube heat exchanger with the designation *9.1-0.737-S*, for which pressure drop and heat transfer correlations were provided by Kays and London [15]. The geometry of this heat exchanger is shown in Fig. 3a) and Fig. 4, and it will be assumed that the pressure drop and heat transfer correlations are applicable for curved fins as well, as illustrated in Fig. 3b). As shown in Table 1, this geometry provides a relatively large *heat transfer surface area to heat exchanger volume ratio* ($\alpha_{air}$) and a high ratio of *free-flow area versus frontal area* ($\sigma_{air}$), for which the former should be beneficial for heat transfer and the latter for the pressure drop. The core air flows between the fins while hydrogen flows inside the pipes with the stadium-shaped cross-section.

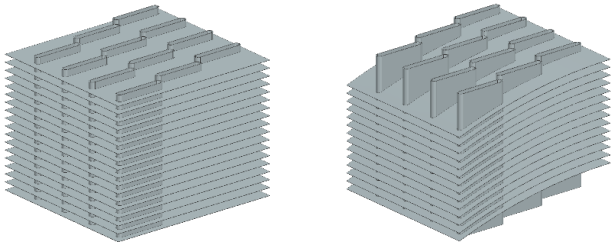


**FIG. 3 – A) BASELINE GEOMETRY OF THE 9.1-0.737-S FINNED FLAT TUBE HEAT EXCHANGER [15] B) MODIFIED GEOMETRY WITH CURVED FINS.**

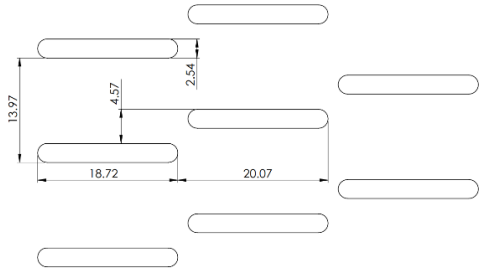


**FIG. 4 – BASELINE HEAT EXCHANGER TUBE SCHEMATIC (IN MILLIMETERS) [15].**

**TABLE 1 - HEAT EXCHANGER 9.1-0.737-S PROPERTIES.**

| 9.1-0.737-S HEX | |
|---|---|
| Free-flow area/frontal area $\sigma_{air}$ | 0.788 |
| Fin area/total area $\xi_{fin}$ | 0.813 |
| Fin spacing [mm] | 2.794 |
| Total air-side transfer area/total volume $\alpha_{air}$ $[m^2/m^3]$ | 734.9 |
| Tube wall thickness [mm] | 0.254 |
| Air-side hydraulic diameter $D_h$ $[mm]$ | 4.206 |

In this paper, the straight fin heat exchanger is treated as a rectangular box for the purpose of aerothermal conceptual design, using the size parameters $L_x$, $L_y$, and $L_z$ according to Fig. 5, which define the total heat exchanger volume and surface areas. The length of the heat exchanger in the air direction $L_x$ is determined by the chosen number of tube banks $N_{banks}$, which has been set based on prior experience, balancing pressure loss, heat transfer, and volume. The length of the heat exchanger in the hydrogen direction, $L_y$, is calculated using the AR for the diffuser duct and radius of the HEX centroid, as shown in Fig. 5. For the curved heat exchangers, the dimensions are kept the same as for the straight fin heat exchanger in order to maintain the same number of tube banks. This effectively leads to more surface area for the fins, which could result in increased heat transfer and skin friction losses. In order to be conservative with respect to aerodynamic performance the curved heat exchanger is assumed to have the same overall heat flow Q as its straight-fin counterpart. Friction losses on the other hand will be

accounted for and will be explained further in section 3.2. During conceptual design the air-side pressure loss is calculated using the following equation from Kays and London [15]:

$$\Delta p_{0,air} = \frac{G_{air}^2}{2\rho_{air,1}}\left((1+\sigma_{air}^2)\left(\frac{\rho_{air,1}}{\rho_{air,2}}-1\right)+f\frac{4L_x}{D_{h,air}}\frac{\rho_{air,1}}{\bar{\rho}_{air}}\right) \quad (1)$$

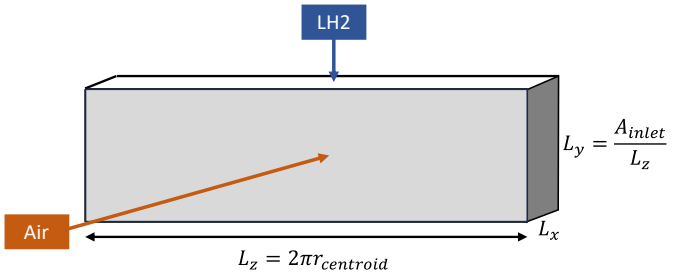


**FIG. 5 - DIMENSIONS OF THE HEAT EXCHANGER FOR CONCEPTUAL DESIGN**

The method used for calculating heat exchanger performance is the effectiveness-number-of-transfer-units ($\epsilon - NTU$) method, which can be found in several textbooks and publications [15,16] and has been implemented in an in-house Python code. The thermophysical properties used in the calculations are obtained from the NIST REFPROP software [17] via the Python wrapper for Coolprop [18], providing highly accurate real fluid/gas properties for the conceptual design process. For the calculations in this paper a dry air mixture has been chosen for the air side while Parahydrogen has been chosen for the hydrogen side of the heat exchanger.

### 3.2 Duct design and aerodynamic optimization

The main design objectives of the duct design are to diffuse the flow uniformly before entering the heat exchanger and to minimize the air-side total pressure drop, thereby resulting in uniform cooling and a low impact on engine performance. The objective functions of the optimization can therefore be stated as 1) minimization of the total pressure drop between the diffuser inlet and contraction outlet (Fig. 2) and 2) the minimization of the flow non-uniformity $\psi$ at the HEX inlet:

$$\psi = \int_{A_{inlet}} |v'|\, dA \Big/ \int_{A_{inlet}} V dA \quad (2)$$

The flow perturbation $v'$ on the heat exchanger inlet is defined as the difference between the velocity at a specific point and the averaged velocity on the HEX inlet surface (see Fig. 2):

$$v' = V - \frac{1}{A_{inlet}} \int_{A_{inlet}} V dA \quad (3)$$

The approach chosen here consists of an aerodynamic optimization campaign which varies the duct design and uses CFD simulations to simulate its performance. The diffuser and contraction ducts are parametrized using Bezier curves, amounting to a total of 12 variables required to define the design, which also includes the inclination of the HEX and the angle between the fins and the HEX inlet.

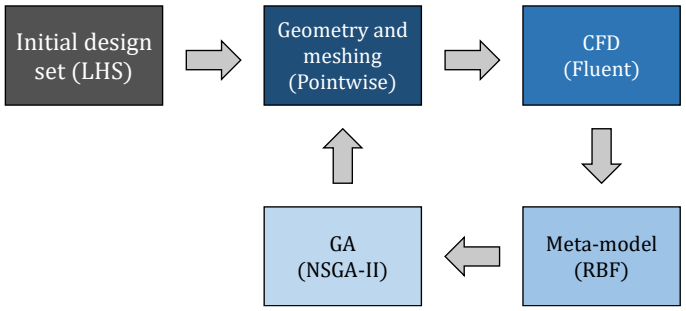


**FIG. 6 - OPTIMIZATION FRAMEWORK**

The optimization framework is outlined in Fig. 6. It starts by creating an initial design set by means of a Latin Hypercube Sampling (LHS), which samples the design space of the duct geometries. These geometries are then meshed and simulated using CFD. The results are postprocessed and the values of the objective functions (total pressure loss and HEX inlet flow non-uniformity) are extracted and used to create a meta-model. This meta-model is then used by the Genetic Algorithm (GA), which finds new designs that minimize the objective functions. In turn, these new designs are meshed, simulated, and added to the meta-model which will be used by the GA once again. This process iterates until no improvement is reached for the objective functions.


**FIG. 7 – LOCATION OF HEX DOMAIN, INLET, AND OUTLET.**

Meshing is carried out using the meshing software Pointwise, which generates 2D computational meshes consisting of unstructured, triangular and quadrilateral cells (see Fig. 7), with cell counts usually fluctuating around 50k-100k cells and adhering to a first node height $y^+$ below 1. CFD simulations are carried out using ANSYS Fluent assuming 2D, axisymmetric conditions and incorporating the $k-\omega$ SST turbulence model. The inlet is defined using total temperature and pressure while a mass flow is prescribed in the outlet. In the present analysis the heat exchanger is not discretely represented, instead it is modeled using a porous media approach. Hence, the pressure drop from the fins and its effect on the flow is modelled through an inertial resistance factor $\lambda$ in the HEX domain (see Fig. 7), similar to other existing heat exchanger studies [19–22]. This factor acts in the direction of the fins, accounting for the streamwise pressure drop in the HEX as formulated in Eq (4), using the total pressure drop from Eq. (1). A value three orders of magnitude greater was also imposed in the transversal direction, thereby forcing the flow along the direction of the fins of the heat exchanger.

$$\lambda = 2\Delta p_{0,air}/\rho_{1,air} v_{1,air}^2 L_x \quad (4)$$

$$v_{1,air} = \dot{m}_{air} / A_{inlet} \rho_{1,air} \quad (5)$$

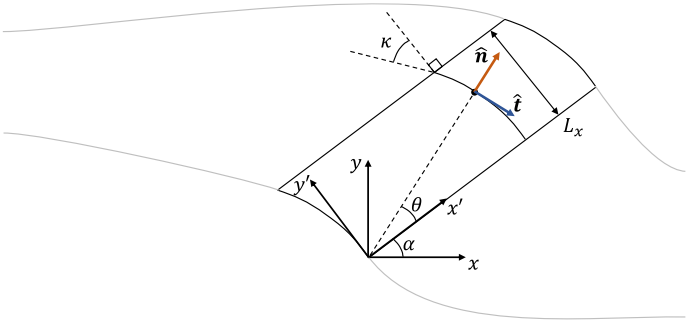


**FIG. 8 – COORDINATE SYSTEM AND DIRECTIONAL VECTORS FOR THE INERTIAL RESISTANCE FACTOR.**

In ANSYS Fluent one needs to specify two directional vectors, $\hat{\boldsymbol{t}}$ which is tangent to the direction of the fin and along which the inertial resistance factor $K$ acts, and a vector $\hat{\boldsymbol{n}}$ normal to the fin surface. For a straight fin heat exchanger this is equivalent to a rotation matrix with the inclination $\alpha$ of the HEX. For the curved fin heat exchanger the fins where defined as circular arcs as shown in Fig. 8. The *fin leading edge angle* $\kappa$ is used to adjust the angle of the fin with respect to the inlet of HEX, while it is assumed that the trailing edge of the fin is perpendicular to the outlet surface of the HEX. With these assumptions one can readily calculate the needed directional vectors. First, a local $x - y$ coordinate system is created with the origin at the intersection between the HEX hub and its outlet, as shown in Fig. 8. In turn, this coordinate system is rotated by the inclination of the HEX $\alpha$ to generate a new $x' - y'$ coordinate system:

$$y' = x \sin\alpha + y \cos\alpha \quad (6)$$

The angle $\theta$ is a function of the coordinate $y'$ and the fin metal angle $\kappa$:

$$\theta = \sin^{-1}\left(\frac{y' \sin\kappa}{L_x}\right) \quad (7)$$

Which can then be used to define the normal $\hat{\boldsymbol{n}}$ and tangential $\hat{\boldsymbol{t}}$ vectors at any location on the curved fin:

$$\hat{\boldsymbol{n}} = \begin{bmatrix} cos(\theta+\alpha) \\ sin(\theta+\alpha) \end{bmatrix} \quad \hat{\boldsymbol{t}} = \begin{bmatrix} \sin(\theta+\alpha) \\ -\cos(\theta+\alpha) \end{bmatrix} \quad (8)$$

Here, it can be seen that for a fin leading edge angle of zero ($\kappa = 0$) the directional vectors correspond to a straight fin geometry. This setup also accounts for the increased skin friction losses due to the larger surface area of curved fins since the flow will take a longer path to cross the HEX compared to a design with straight fins. For this paper, designs will be analyzed for fin leading edge angles $\kappa$ of 0° (straight fins), 20°, and 40° degrees (curved fins).

Heat transfer was incorporated into the CFD model by using the energy source term $\dot{q}$ in Eq. (9) that acts as a heat sink in the HEX domain:

$$\dot{q} = Q / V_{HEX} \quad [\mathrm{W/m^3}] \quad (9)$$

# 4 RESULTS

## 4.1 Heat exchanger conceptual design

The integrated ICD heat exchanger has been designed for a hydrogen engine in the 30,000 lbf thrust class, year 2050, geared turbofan for short-medium range (SMR) applications. This base engine model has been previously presented in [14] by the authors, where its technology parameters and engine performance can be found. It should be noted that this engine itself does not feature intercooling but serves as a basis for the design of the ICD and compact heat exchanger. Values extracted from this engine model serve as boundary conditions for the heat exchanger conceptual design and are included in Table 2, which together with the heat exchanger design parameters in Table 3 define the design.

**TABLE 2 – ICD BOUNDARY CONDITIONS.**

| Air-side | TO | ToC | Cruise |
|---|---|---|---|
| Mass flow [kg/s] | 28.86 | 12.91 | 11.25 |
| LPC outlet area | 0.0807 | 0.0807 | 0.0807 |
| LPC outlet Mach number | 0.3831 | 0.3997 | 0.3819 |
| $p_0$ [MPa] | 0.2909 | 0.1189 | 0.1057 |
| $T_0$ [K] | 398.2 | 356.7 | 344.1 |
| **H2-side** | **TO** | **ToC** | **Cruise** |
| Fuel flow [kg/s] | 0.3143 | 0.1278 | 0.1022 |
| $p_0$ [MPa] | 4.200 | 1.863 | 1.571 |
| $T_0$ [K] | 26.66 | 24.31 | 24.07 |

The length of the ICD is set using the parameter $\Delta R/L$ (Fig. 2) which relates change in mid-radius to the length of the duct from the inlet to the outlet, with higher values being representative of shorter, more aggressive duct designs [23]. The value chosen here allows for accommodating the volume of the compact heat exchanger. As mentioned earlier, the number of tube banks $N_{banks}$ determines the length of the HEX in the air direction and has been set based on prior experience, balancing pressure loss, heat transfer, and volume. The chosen thermal conductivity $k$ is representative for aluminum alloys of the 2, 5, and 7 series which could serve as suitable structural materials from a heat transfer perspective. The heat exchanger matrix geometry, provided in the literature, is scaled down isometrically by 50% in order to decrease the air-side Reynolds number, increase the Nusselt number, and increase the heat transfer surface area to heat exchanger volume ratio ($\alpha_{air}$). The tube wall thickness has also been increased compared to the baseline geometry in order to increase the hydrogen-side flow velocities and heat transfer.

**TABLE 3 –INPUT PARAMETERS FOR THE COMPACT HEAT EXCHANGER CONCEPTUAL DESIGN.**

| HEX design parameters | |
|---|---|
| $\Delta R/L$ | 0.2 |
| $N_{banks}$ | 8 |
| $k\ [W/m\,K]$ | 120 |
| Tube wall thickness [mm] | 0.508 |

The cryogenic temperatures of the fuel can potentially cause the elements of the air to condense or even freeze in the heat exchanger surface. One way to control the heat exchanger surface temperature is to recirculate the pre-heated hydrogen, as

examplified in Fig. 9. Hence, 50% of the mass flow in the heat exchanger outlet is recirculated back and mixed with the incoming, colder hydrogen at the heat exchanger inlet. For the present case this allows to keep the air-side temperature above the nitrogen condensing and freezing temperatures. However, in the presence of humid air, the temperature should be kept above the water freezing point, which can be accomplished by increasing the level of recirculation.

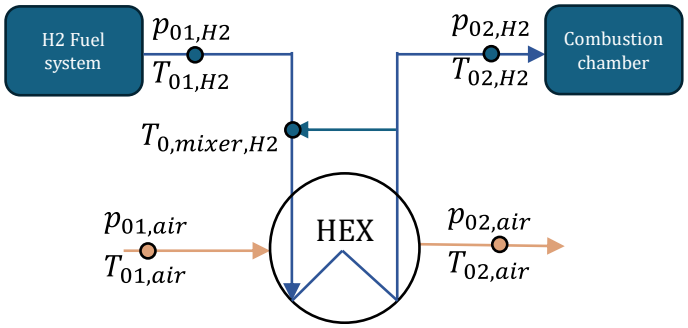


**FIG. 9 – LAYOUT OF RECIRCULATION SYSTEM**

The aerothermal performance of the heat exchanger is shown for three operating points in Table 4, where top-of-climb (ToC) has been chosen as the design point. This is due to the high LPC outlet Mach numbers, which will make this the most challenging operating point for the diffuser duct design.

**TABLE 4 - HEX AEROTHERMAL PERFORMANCE. WEIGHT INCLUDES ONLY THE HEAT EXCHANGER MATRIX GEOMETRY. CHANGES IN TEMPERATURE AND PRESSURE ARE CALCULATED USING THE STATIONS IN FIG. 9.**

| | TO | ToC | Cruise |
|---|---|---|---|
| $Q$ [kW] | 1515 | 602 | 474 |
| $L_x$ [m] | 0.08 | 0.08 | 0.08 |
| $L_y$ [m] | 0.26 | 0.26 | 0.26 |
| $T_{0,H2,mixer}$ [K] | 127 | 121 | 119 |
| $\Delta T_{0,air}$ [K] | -51.9 | -46.3 | -41.8 |
| $\Delta T_{0,H2}$ [K] | +304 | +296 | +291 |
| $\Delta p_{0,air}/p_{01}$ | 1.5% | 2.0% | 2.0% |
| $\Delta p_{0,H2}/p_{01,H2}$ | 2.6% | 2.7% | 2.5% |
| W [kg] | 12.1 | 12.1 | 12.1 |
| $\epsilon$ | 82% | 89% | 91% |

Relatively large heat flows have been achieved, especially during take-off (TO), where the air-side temperature drop has reached 53 K due to a combination of high core air mass flow, pressure, and temperature. The incurred total pressure drops are relatively modest but only represent the losses occurring in the heat exchanger matrix itself and for now exclude the losses in the diffuser duct, contraction duct, and hydrogen piping.

Recirculation has led to hydrogen inlet temperatures (after mixing) between 119 and 127 K, well above the condensation temperatures of nitrogen, oxygen, and argon, which constitute 99.97% of Earth's atmosphere [24].

The size, heat flow, HEX pressure drop, and the fluid inlet temperatures and pressures of the ICD will be used in the next section to generate and optimize duct designs.

## 4.2 Duct design and optimization

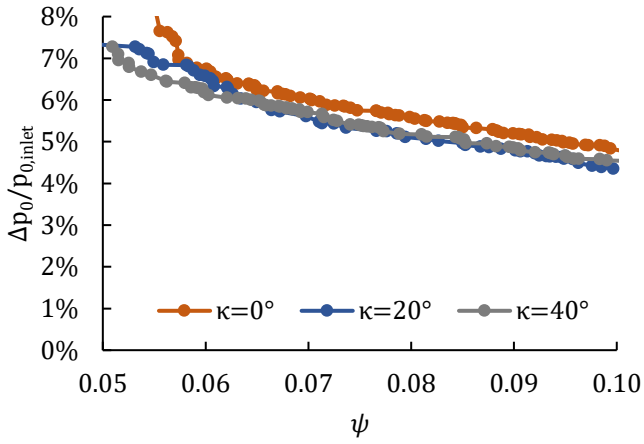


**FIG. 10 – PARETO FRONTS OF TOTAL PRESSURE DROP VERSUS FLOW NON-UNIFORMITY FOR THE THREE OPTIMIZATION ATTEMPS CARRIED OUT.**

The duct shape optimization campaign encompasses three separate optimization efforts, including for straight fins ($\kappa = 0°$) and curved fins ($\kappa = 20°$ and $40°$). Each attempt amounted to more than 2000 different duct designs which were all simulated using CFD. The resulting pareto fronts with respect to total pressure drop and flow non-uniformity are shown in Fig. 10. As can be seen the integrated curved fin heat exchangers operate with lower overall total pressure drops than their straight fin counterparts.

Table 5 contains a set of integrated duct designs which have been selected for further analysis, representing low ($\psi = 0.055$), medium ($\psi = 0.08$), and high ($\psi = 0.1$) flow non-uniformity at the HEX inlet. The three straight fin designs from this table have been plotted in Fig. 11 in terms of Mach number contours and seem to indicate that lower overall pressure drops result from longer diffusers, resulting in lower HEX inlet velocities but also increased flow non-uniformity. The latter is primarily due to boundary layer thickening in the diffuser hub and shroud, which is particularly noticeable at the diffuser shroud for design 1196 and 695 (see Fig. 11). Besides the boundary layer thickening the flow remains attached with no boundary layer separation. Here it can be seen that largest improvement in total pressure drop is present for cases with low flow non-uniformity, e.g. comparing design 1784 with 1880 in Table 5, which shows a decrease in total pressure drop from 7.63% to 6.48%.

**TABLE 5 – CHOSEN DESIGNS FROM THE PARETO FRONTS FOR FURTHER ANALYSIS.**

| Design: | 1784 | 1196 | 695 | 2058 | 1678 | 1662 | 1880 | 1253 | 1969 |
|---|---|---|---|---|---|---|---|---|---|
| $\kappa$ | 0 | 0 | 0 | 20 | 20 | 20 | 40 | 40 | 40 |
| $\Delta p_0/p_{0,inlet}$ | 7.63% | 5.60% | 4.80% | 6.84% | 5.12% | 4.35% | 6.48% | 5.20% | 4.57% |
| $\psi$ | 0.055 | 0.08 | 0.1 | 0.055 | 0.08 | 0.1 | 0.055 | 0.08 | 0.1 |

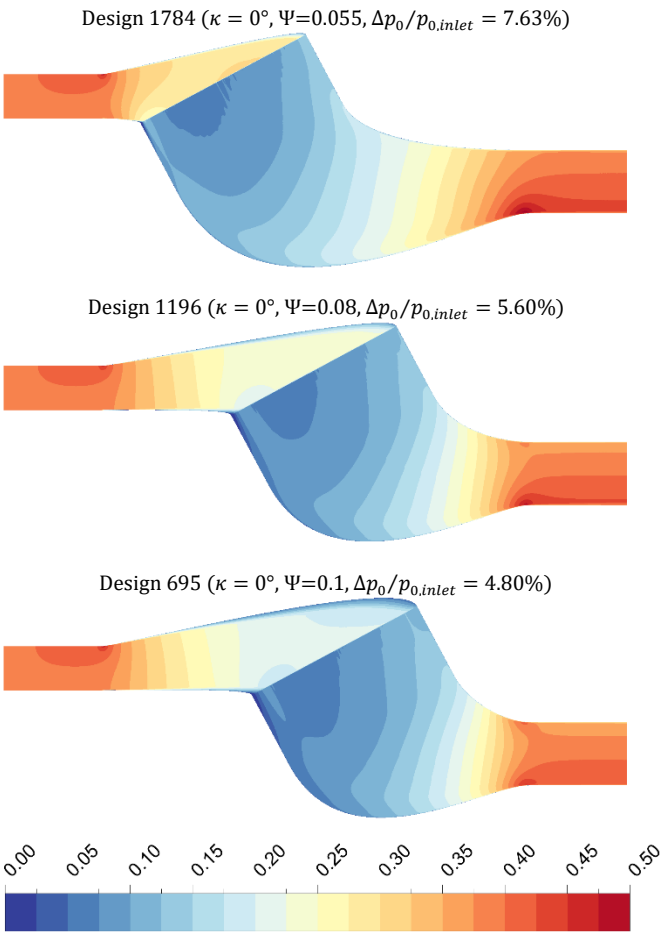


**FIG. 11 – MACH NUMBER DISTRIBUTION FOR THREE DESIGNS WITH STRAIGHT FINS AND INCREASEING NON-UNIFORMITY $\psi$.**

The effect of the curved fins on the flow can be seen in Fig. 13 for a straight fin design and two curved designs (20° and 40°) for a flow non-uniformity of $\psi = 0.08$. The flow in the diffuser is very similar for all designs, and the average velocity just upstream of the HEX inlet (station 2 Fig. 12) ranges from 83 to 85 m/s for all three designs. Just downstream of the HEX (station 3 Fig. 12) the flow velocities are markedly higher for the curved cases (see Fig. 13), resulting in an average velocity of 46 m/s for design 1253 ($\kappa = 40°$) compared to 33 m/s for the straight fin design 1196. These findings indicate that there is a much less sudden deceleration of the flow at the HEX inlet for the curved fin heat exchangers compared to the straight fin designs.

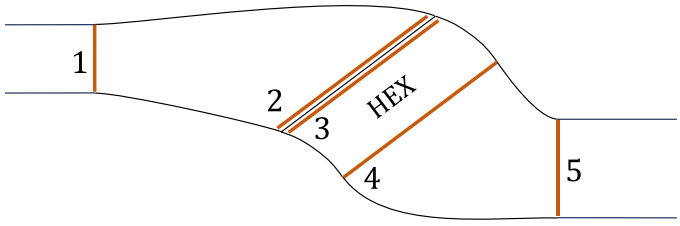


**FIG. 12 – STATION NUMBERING (BRONZE LINES) USED FOR CALCULATING LOSS COMPOSITION.**

The loss composition in the integrated heat exchangers and ducts will now be examined in more detail in Fig. 14 for the cases in Table 5. As before, one can see that the total pressure drop $\Delta p_0/p_{0,inlet}$ (from station 1 to 5 in Fig. 12) decreases for increased flow non-uniformity. If this is subdivided further one can also see that the smallest pressure drops for all the presented cases can be found in the diffuser (from station 1 to 2) and contraction (station 4 to 5).

The velocity in the HEX inlet face can be decomposed into two components, one parallel to the fins at the HEX inlet, and one in the transversal direction. The kinetic energy of the later component is named the *transversal kinetic energy* and is the largest loss source for the straight finned HEX designs due to large incidence angles at the leading edge of the fins. It is evaluated at station 2 in Fig. 12. For the curved fin designs this loss is significantly lower, but these designs instead feature higher total pressure losses in the HEX itself due to longer flow paths and higher flow velocities in the HEX compared to the straight fin designs. From the results presented here it can be observed that the curved fins yield the largest reductions in pressure drop for cases where low flow non-uniformity or a shorter diffuser duct length is desired.

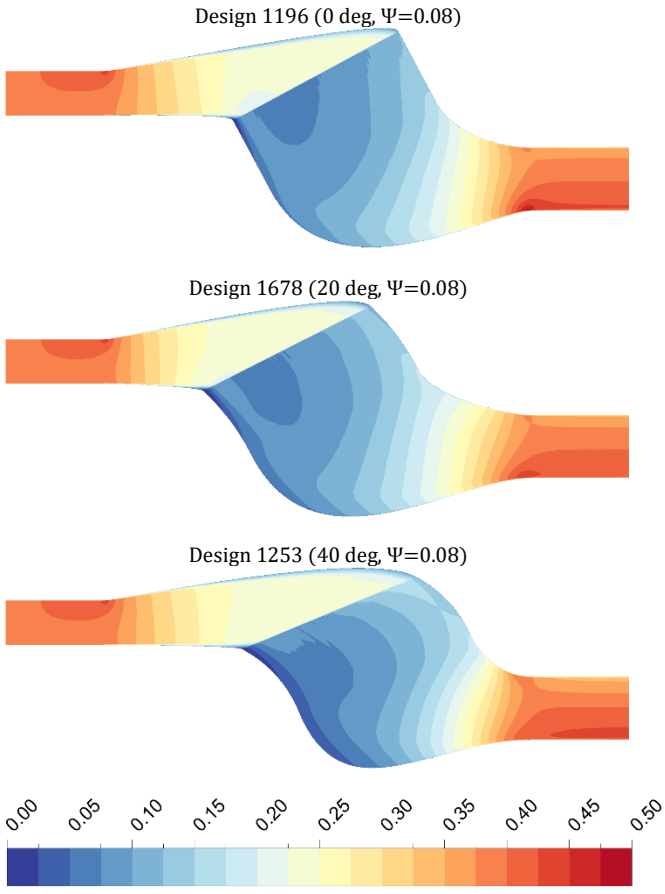


**FIG. 13 – MACH NUMBER DISTRIBUTION FOR THREE CHOSEN DESIGNS AT FLOW NON-UNIFORMITY $\psi = 0.08$.**

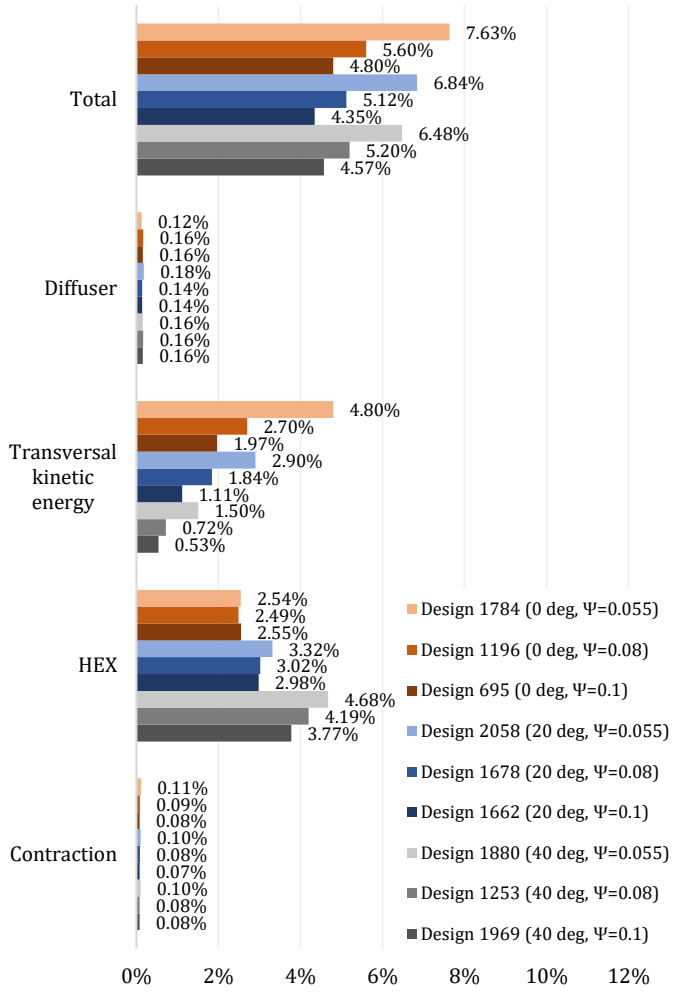


**FIG. 14 – BREAKDOWN OF TOTAL PRESSURE LOSSES. EACH COLOR GROUP REPRESENTS EITHER 0, 20, OR 40 DEGREES OF FIN LEADING EDGE ANGLE $\kappa$. WITHIN EACH GROUP THE FLOW NON-UNIFORMITY $\psi$ INCREASES WITH THE SHADING OF EACH COLOR.**

### 4.3 Pressure loss correlations

From Table 5 an integrated duct and heat exchanger geometry was chosen which strikes a balance between total pressure loss and flow non-uniformity, design 1662, featuring a fin leading edge angle of 20° and the lowest total pressure loss of the presented designs. The pressure loss correlations will be based on data from a series of CFD simulations where the dynamic viscosity of the air has been varied to obtain different duct Reynolds numbers $Re_{D_h}$. The mesh was refined in accordance with a previously published mesh study by the authors [14] resulting in a mesh cell count of 337k cells. The remaining CFD setup is identical to the one described in section 3.2.

The pressure loss coefficient $K_{ICD}$ is defined as the total pressure loss between the diffuser inlet (station 1 in Fig. 12) and the contraction outlet (station 5), normalized with the dynamic pressure at the diffuser inlet:

$$K_{ICD} = \frac{p_{01} - p_{05}}{p_{01} - p_1} = 0.5106 Re_{D_h}^{-0.01624} + \frac{2415}{Re_{D_h}} \quad (10)$$

The range of applicability is $10^5 < Re_{D_h} < 4 \cdot 10^6$ with a maximum error of 0.05% compared to the underlying CFD simulation data. The correlation is also plotted in Fig. 15. The Reynolds number is calculated using a hydraulic diameter defined using the diffuser inlet hub and shroud diameters:

$$D_h = D_{1,shroud} - D_{1,hub} \quad (11)$$

The presented pressure loss correlation can be readily incorporated into future engine system level simulations, similar to existing work on intercooling and recuperation [14,25].

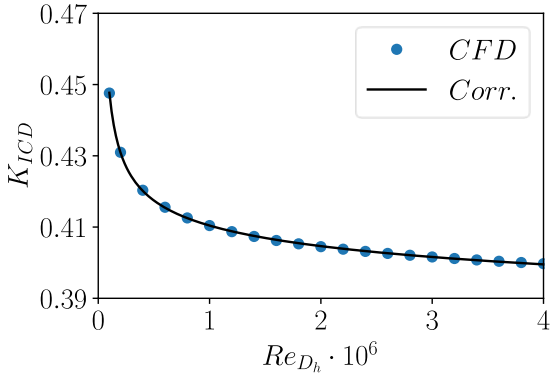


**FIG. 15 – PRESSURE LOSS CORRELATION FOR THE INTEGRATED DUCT AND HEAT EXCHANGER DESIGN 1662.**

### 4.4 Simulation with discrete fins

This section aims to compare the porous media approach used during the optimization with a CFD simulation of a case containing discrete fins which are included in the computational mesh. For the case of straight fins, a verification case was presented in a previous paper by the authors [14]. There, the tubes of the heat exchanger geometry were omitted from the model to keep the case 2D and the computational mesh at a manageable size. The results showed very good agreement between the porous media and discrete fin approaches with respect to velocity and pressure profiles at the HEX and contraction outlets. The results asserted the choice of employing the porous media approach for the purpose of aerodynamic optimization.

In this paper the aim was to verify case 1662 using the same methodology and mesh settings which were employed and verified in the previous paper [14]. The inlet is defined using total temperature and pressure while a mass flow is prescribed in the outlet (see Table 2), the same as for the porous media cases described in section 3.2. All walls are set as adiabatic except for the fins which have a prescribed heat flux. When simulating this case, it was found that the low momentum boundary layer flow of the diffuser hub had led to a cold spot in the heat exchanger matrix, as has been visualized in Fig. 16. An additional factor contributing to this effect is that the discrete fin simulation does not allow for heat to flow between the fins while it is possible in

the porous media simulations. This explains why the cold spot was not as severe in that case.

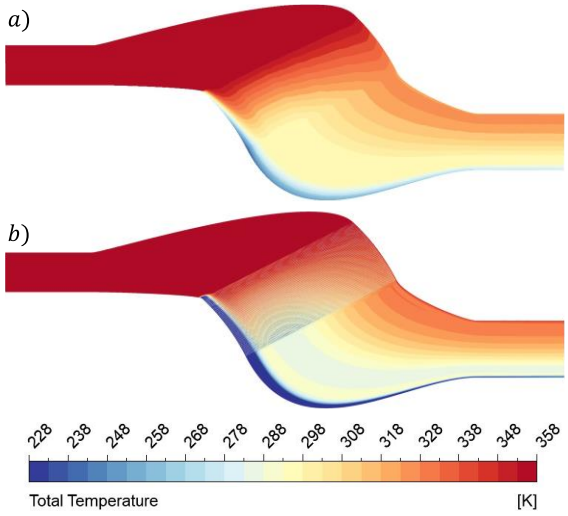


**FIG. 16 – TOTAL TEMPERATURE CONTOURS FOR THE A) POROUS MEDIA SIMULATION AND B) DISCRETE FIN SIMULATION FOR CASE 1662. THE TEMPERATURES IN THE COLD SPOT APPROACHED THE LOWER LIMIT SET IN THE CFD SOLVER (100 K).**

For a fully detailed HEX geometry, including the hydrogen inflow placed at the HEX shroud, tubes, and an outlet at the HEX hub, the cold spot at the diffuser hub will be much less pronounced since the hydrogen at this location will already have been heated to ~320 K, which is the hydrogen outlet temperature according to Table 4 (for ToC). Therefore, the pressure loss correlation given in Eq. (10) is still applicable for use in system-level engine studies.

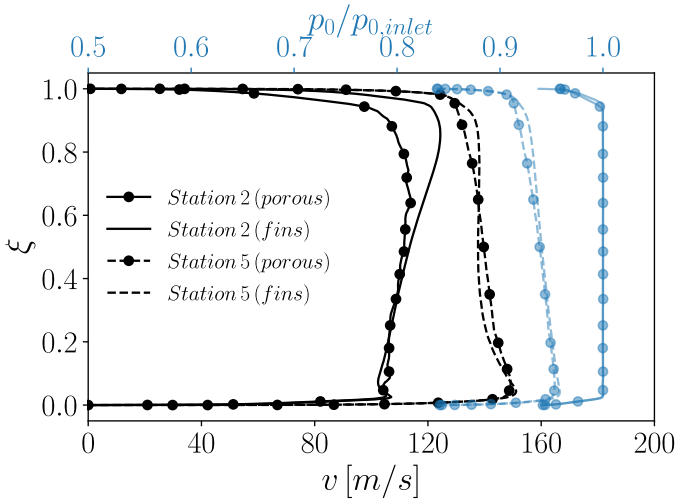


**FIG. 17 – VELOCITY (BLACK) AND TOTAL PRESSURE (BLUE) PROFILES AT STATION 2 AND 5 (SEE FIG. 12) AS FUNCTION OF DIMENSIONLESS DISTANCE $\xi$ FROM HUB TO SHROUD.**

The cold spot was observed for all cases in Table 5 with medium and high flow non-uniformity. On the other hand, the low non-uniformity cases did not feature this cold spot, which highlights the need for the designer to be aware of this risk and to check the design with increasingly more detailed analyses and/or adapt the design further.

To provide a reasonable verification the choice fell on case 1880, which does not feature the same type of cold spot as was found for case 1662. Velocity and total pressure profiles have been extracted at station 2 and 5 in Fig. 12, corresponding to the diffuser outlet and contraction outlet, and show good agreement between the two simulation approaches. The velocity is higher closer to the shroud for the discrete fin approach compared to porous media approach, but the remaining profiles match relatively well. This comparison has again shown that the employed source term approach offers a computationally cheap and sufficiently accurate approach for the purpose of aerodynamic optimization.

## 5 CONCLUSIONS

This paper has presented results for the conceptual design and aerodynamic optimization of a compact heat exchanger integrated with an ICD. The heat exchanger features curved fins instead of the more conventional straight fins to improve flow turning and decrease pressure losses.

Conceptual design of the heat exchanger shows the capability of achieving relatively large heat flows (up to 1.5 MW) while keeping a relatively compact format. Already heated hydrogen from the HEX outlet is recirculated back to the inlet to increase the hydrogen inlet temperature to avoid condensation of nitrogen and hydrogen on the air-side of the HEX.

Aerodynamic optimization of the integrated ducts has resulted in a design which has significantly decreased total pressure losses compared to a straight fin design.

The benefit of using a curved fin heat exchanger is more pronounced when a shorter diffuser or lower flow non-uniformity is desired. If longer diffusers are used then the velocities at the heat exchanger inlet are decreased, which will lead to lower transversal kinetic energy losses at the leading edge of the fins. It was also found that the total pressure loss inside the HEX itself is higher for the curved designs due to longer flow paths and higher flow velocities.

A pressure loss correlation was generated for an integrated curved fin heat exchanger for future use in engine system level calculations. This will allow for quantifying the effect on fuel consumption and emissions.

## 6 ACKNOWLEDGEMENTS

The work was financed and supported by Chalmers' Areas of Advance Transport project “PATH - Pathways for a sustainable introduction of hydrogen into the aviation sector” and the Competence Centre TechForH2. Support was also provided by the project MINIMAL (Minimum environmental impact ultra-efficient cores for aircraft propulsion). The MINIMAL project is co-funded by the European Union’s Horizon Europe Programme under the grant agreement n°101056863 and by the UK Research and Innovation (UKRI) funding guarantee under the project reference n° 10040930, 10053292 and 10039071. Additional funding is provided by GKN Aerospace Sweden AB. The simulations were enabled by resources provided by the National Academic Infrastructure for

Supercomputing in Sweden (NAISS) and the Swedish National Infrastructure for Computing (SNIC) at C3SE partially funded by the Swedish Research Council through grant agreements no. 2022-06725 and no. 2018-05973.

## 7 REFERENCES

[1] European Commision, Communication From The Commission To The European Parliament, The European Council, The Council, The European Economic And Social Committee And The Committee Of The Regions-The European Green Deal., (2019) 1. https://eur-lex.europa.eu/legal-content/EN/TXT/?uri=COM:2019:640:FIN.

[2] Hydrogen Europe, Hydrogen Europe, (n.d.). https://hydrogeneurope.eu/clean-h2-partnership-issues-195m-call/.

[3] E. Partnership, H. Europe, European Partnership under Horizon Europe Clean Aviation, (2020). https://www.era-learn.eu/documents/final_report_ms_partnerships.pdf.

[4] E.J. Adler, J.R.R.A. Martins, Hydrogen-Powered Aircraft: Fundamental Concepts, Key Technologies, and Environmental Impacts, Fuel. 32 (2022) 7.

[5] G.D. Brewer, Hydrogen aircraft technology, 2017. https://doi.org/10.1201/9780203751480.

[6] S. Boggia, A. Jackson, Some Unconventional Aero Gas Turbines Using Hydrogen Fuel, in: Vol. 2 Turbo Expo 2002, Parts A B, ASMEDC, 2002: pp. 683–690. https://doi.org/10.1115/GT2002-30412.

[7] I.P. van Dijk, A.G. Rao, J.P. van Buijtene, Stator Cooling & Hydrogen Based Cycle, in: International Symposium on Air Breathing Engines 2009, Montreal, 2009.

[8] F. Svensson, R. Singh, Effects of Using Hydrogen on Aero Gas Turbine Pollutant Emissions, Performance and Design, in: Vol. 2 Turbo Expo 2004, ASMEDC, 2004: pp. 107–116. https://doi.org/10.1115/GT2004-53349.

[9] A. Capitao Patrao, I. Jonsson, C. Xisto, A. Lundbladh, M. Lejon, T. Grönstedt, The heat transfer potential of compressor vanes on a hydrogen fueled turbofan engine, Appl. Therm. Eng. 236 (2024) 121722. https://doi.org/10.1016/j.applthermaleng.2023.121722.

[10] D. Jian, Z. Qiuru, Key technologies for thermodynamic cycle of precooled engines: A review, Acta Astronaut. 177 (2020) 299–312. https://doi.org/10.1016/j.actaastro.2020.07.039.

[11] H. Abedi, C. Xisto, I. Jonsson, T. Grönstedt, A. Rolt, Preliminary Analysis of Compression System Integrated Heat Management Concepts Using LH2-Based Parametric Gas Turbine Model, Aerospace. 9 (2022). https://doi.org/10.3390/aerospace9040216.

[12] J.J. Murray, A. Guha, A. Bond, Overview of the development of heat exchangers for use in air-breathing propulsion pre-coolers, Acta Astronaut. 41 (1997) 723–729. https://doi.org/10.1016/S0094-5765(97)00199-9.

[13] I. Jonsson, C. Xisto, H. Abedi, T. Grönstedt, M. Lejon, Feasibility study of a radical vane-integrated heat exchanger for turbofan engine applications, in: Proc. ASME Turbo Expo, American Society of Mechanical Engineers, 2020: pp. 1–8. https://doi.org/10.1115/GT2020-15243.

[14] A.C. Patrao, I. Jonsson, C. Xisto, A. Lundbladh, T. Grönstedt, Compact heat exchangers for hydrogen-fueled aero engine intercooling and recuperation, Appl. Therm. Eng. 243 (2024) 122538. https://doi.org/10.1016/j.applthermaleng.2024.122538.

[15] W.M. Kays, A.L. London, Compact Heat Exchangers, 2nd ed., McGraw-Hill, 1984.

[16] F.P. Incropera, D.P. DeWitt, T.L. Bergman, A.S. Lavine, Fundamentals of Heat and Mass Transfer, 6th ed., Wiley, New York, 2007.

[17] E.W. Lemmon, I.H. Bell, M. Huber, M. McLinden, NIST standard reference database 23: reference fluid thermodynamic and transport properties - REFPROP, version 10.0, (2018).

[18] I.H. Bell, J. Wronski, S. Quoilin, V. Lemort, Pure and Pseudo-pure Fluid Thermophysical Property Evaluation and the Open-Source Thermophysical Property Library CoolProp, Ind. Eng. Chem. Res. 53 (2014) 2498–2508. https://doi.org/10.1021/ie4033999.

[19] D. Missirlis, K. Yakinthos, A. Palikaras, K. Katheder, A. Goulas, Experimental and numerical investigation of the flow field through a heat exchanger for aero-engine applications, Int. J. Heat Fluid Flow. 26 (2005) 440–458. https://doi.org/10.1016/j.ijheatfluidflow.2004.10.003.

[20] K. Yakinthos, D. Missirlis, A. Palikaras, P. Storm, B. Simon, A. Goulas, Optimization of the design of recuperative heat exchangers in the exhaust nozzle of an aero engine, Appl. Math. Model. 31 (2007) 2524–2541. https://doi.org/10.1016/j.apm.2006.10.008.

[21] X. Zhao, T. Grönstedt, Conceptual design of a two-pass cross-flow aeroengine intercooler, Proc. Inst. Mech. Eng. Part G J. Aerosp. Eng. 229 (2015) 2006–2023. https://doi.org/10.1177/0954410014563587.

[22] D. Misirlis, Z. Vlahostergios, M. Flouros, C. Salpingidou, S. Donnerhack, A. Goulas, K. Yakinthos, Optimization of heat exchangers for intercooled recuperated Aero Engines, Aerospace. 4 (2017). https://doi.org/10.3390/aerospace4010014.

[23] C.O. Dueñas, R.J. Miller, H.P. Hodson, J.P. Longley, Effect of length on compressor inter-stage duct performance, Proc. ASME Turbo Expo. 6 PART A (2007) 319–329. https://doi.org/10.1115/GT2007-27752.

[24] D.R. Lide, CRC handbook of chemistry and physics, CRC press, 2004.

[25] X. Zhao, O. Thulin, T. Grönstedt, First and Second Law Analysis of Intercooled Turbofan Engine, J. Eng. Gas Turbines Power. 138 (2015). https://doi.org/10.1115/1.4031316.

 